Inactivating negative regulators of cortical branched actin enhances persistence of single cell migration

Artem I Fokin, Arthur Boutillon, John James, Laura Courtois, Sophie Vacher, Gleb Simanov, Yanan Wang, Anna Polesskaya, Ivan Bièche, Nicolas B David, et al.

Inactivating Negative Regulators of Cortical Branched Actin Enhances Persistence of Single Cell Migration

Artem I. Fokin[1,*], Arthur Boutillon[2,–], John James[1], Laura Courtois[3], Sophie Vacher[3], Gleb Simanov[1,–], Yanan Wang[1,–], Anna Polesskaya[1], Ivan Bièche[3], Nicolas B. David[2], Alexis M. Gautreau[1,*]

[1] CNRS UMR7654, Ecole Polytechnique, Institut Polytechnique de Paris, 91120 Palaiseau, France

[2] INSERM U1182, CNRS UMR7645, Ecole Polytechnique, Institut Polytechnique de Paris, 91120 Palaiseau, France

[3] Pharmacogenomics Unit, Department of Genetics, Institut Curie, 26 rue d'Ulm, 75005 Paris, France

– Current addresses:

AB Cluster of Excellence Physics of Life, TU Dresden, Germany

GS INSERM U981, Institut Gustave Roussy, 94805 Villejuif Cedex, France

YW Altos Labs, Cambridge Institute of Science, Cambridge, UK

* Correspondence should be addressed to AIF: artem.fokin@polytechnique.edu

or AMG: alexis.gautreau@polytechnique.edu

Keywords: Cell migration, Migration persistence, Arp2/3, Branched actin, Vimentin.

Abbreviations: Cortical Branched Actin (CBA), Knock-Out (KO), Knock-Down (KD), insertion/deletion (indel), Open Reading Frame (ORF), Mean Square Displacement (MSD), epithelial-mesenchymal transition (EMT), Nucleation Promoting Factor (NPF), Standard deviation (s.d.), Standard-error-to-mean (s.e.m.).

ABSTRACT

The Rac1-WAVE-Arp2/3 pathway pushes the plasma membrane by polymerizing branched actin, thereby powering membrane protrusions that mediate cell migration. Here, using knock-down (KD) or knock-out (KO), we combine the inactivation of the Arp2/3 inhibitory protein Arpin, the Arp2/3 subunit ARPC1A and the WAVE complex subunit, CYFIP2, that all enhance the polymerization of cortical branched actin (CBA). Inactivation of the 3 CBA negative regulators increases migration persistence of human breast MCF10A cells, and of endodermal cells in the zebrafish embryo, significantly more than any single or double inactivation. In the triple KO, but not triple KD cells, the "super-migrator" phenotype was associated with a heterogenous down-regulation of vimentin expression and a lack of coordination in collective behaviors, such as wound healing and acinus morphogenesis. Re-expression of vimentin in triple KO cells restored to a large extent normal persistence of single cell migration, suggesting that vimentin down-regulation contributes to the maintenance of the super-migrator phenotype in triple KO cells. Constant excessive production of branched actin at the cell cortex thus commits cells into a motile state through changes in gene expression.

INTRODUCTION

Cell migration is a critical physiological process during embryo morphogenesis, especially during gastrulation, and in some cell types of the adult, such as immune cells patrolling the organism. Most adult cells, however, do not migrate. They, nonetheless, can be induced to migrate in pathological conditions, for example during cancer progression. Untransformed cells classically use the mesenchymal mode of cell migration that relies on the formation of adherent membrane protrusions called lamellipodia. Lamellipodia are powered by polymerization of branched actin by the Arp2/3 complex (Ridley, 2011; Wu et al., 2012). Several families of Nucleation-Promoting Factors (NPFs) activate the Arp2/3 at different subcellular locations. At the plasma membrane of mammalian cells, the most important families of NPFs are the WAVE family, comprising 3 paralogous proteins, WAVE1, WAVE2 and WAVE3, and the N-WASP family, comprising WASP and N-WASP (Molinie and Gautreau, 2018). For cell migration, WAVE family proteins play a central role in lamellipodium formation, with a variable contribution of N-WASP family proteins depending on the exact cell system (Bieling and Rottner, 2023).

WAVE family proteins are embedded into a multiprotein complex, which is activated by the small GTPase Rac1 at the leading edge of mammalian cells (Ding et al., 2022; Rottner et al., 2021). The control of branched actin polymerization by Rac1 is central in many cell systems, and was for example reported to control cell migration of endodermal cells in the zebrafish embryo during gastrulation (Woo et al., 2012; Giger and David, 2017). Moreover, branched actin is thought to feedback on Rac1 activation and thus to sustain polymerization of branched actin where it was previously polymerized (Castro-Castro et al., 2011; Krause and Gautreau, 2014). Thereby the Rac1-WAVE-Arp2/3 pathway controls persistence of cell migration.

Many proteins inhibit the Rac1-WAVE-Arp2/3 pathway at different levels. Arp2/3 activation can be blocked by several Arp2/3 inhibitory proteins (Chánez-Paredes et al., 2019; Zhao et al., 2020). Arpin occupies one of the two NPF binding sites of Arp2/3 and thus prevents WAVE from activating it (Fregoso et al., 2022). Therefore, Arpin depletion by KD or KO

promotes migration persistence (Dang et al., 2013; Simanov et al., 2021). Branched actin networks can also be debranched by coronins and GMF family proteins that recognize Arp2/3 at the branched junction (Molinie and Gautreau, 2018). The WAVE regulatory complex is inhibited by the Nance-Horan Syndrome family protein NHSL1 that interacts with the WAVE complex and can even replace WAVE in its complex (Law et al., 2021; Wang et al., 2022). Specific GTPase activating proteins inhibit the small GTPase Rac1 to restrict lamellipodial protrusions and cell migration (Parrini et al., 2011; Yamazaki et al., 2013). The ability of GTP-bound Rac1 to activate the WAVE regulatory complex is restricted by CYRI proteins that compete with WAVE complexes for Rac1 binding (Fort et al., 2018; Yelland et al., 2021).

The combinatorial complexity in the assembly of WAVE and Arp2/3 complexes provides additional means to regulate membrane protrusions and cell migration. The paralogous subunits ARPC1B and ARPC5L assemble Arp2/3 complexes that are more active than the ones assembled with ARPC1A and ARPC5 (Abella et al., 2016). We have previously shown that depletion of ARPC1A allows the assembly of more ARPC1B-containing complexes, because common subunits are no longer distributed between the two paralogous proteins, and that ARPC1B-containing Arp2/3 complexes promote cortical branched actin and migration persistence (Molinie et al., 2019). Similarly, we have shown that the CYFIP2-containing WAVE complexes are less readily activated by Rac1 than CYFIP1-containing WAVE complexes and that CYFIP2-depleted cells display increased lamellipodial protrusions and migration persistence (Polesskaya et al., 2022). Because of this balance of paralogous subunits, ARPC1A and CYFIP2 exhibit an apparent inhibitory activity on membrane protrusion and migration persistence, even though these subunits belong to complexes that promote branched actin polymerization. Cortical branched actin polymerized by the Rac1-WAVE-Arp2/3 pathway does not only control cell migration, but also the decision to enter a new cell cycle. In single cells, migration persistence was found to inversely correlate with the duration of the G1 phase (Molinie et al., 2019).

In epithelial cells, cell-cell junctions also depend on the Rac1-WAVE-Arp2/3 pathway for their assembly and maintenance (Li et al., 2020; Verma et al., 2012). When cells reach a high density, they suppress migration and proliferation (Puliafito et al., 2012; Streichan et al., 2014).

Upon wounding the monolayer, cells resume migration and proliferation to heal the wound in a coordinated manner regulated in time and space (Palamidessi et al., 2019; Poujade et al., 2007). Because of this coordination between cells, wound healing is a more complex process than single cell migration. Epithelial cells can also detach from each other through an Epithelial to Mesenchymal Transition (EMT) that relies on changes of gene expression (Thiery et al., 2009). It appeared that there are multiple partial EMT states that determine migration modes (Nieto et al., 2016). Vimentin is an intermediate filament protein that is a marker of EMT. It is initially widely expressed in the embryo and becomes restricted to mesenchymal cells (Paulin et al., 2022). Vimentin is involved in cell migration and appears critical for wound healing in vivo (Eckes et al., 1998; Eckes et al., 2000).

An important question is thus how negative regulators of WAVE-dependent polymerization of branched actin maintain the migration of epithelial cells under control. Here we show that enhancing polymerization of branched actin at the cell cortex by removing as many as 3 negative regulators promotes single cell migration, but not collective migration of mammary epithelial cells. Cells adapt to these long-term perturbations by altering gene expression, in particular, by down-regulating vimentin expression. Vimentin down-regulation enhances migration persistence of single epithelial cells.

RESULTS

Knocking-out 3 CBA negative regulators greatly increases migration persistence

We recently characterized the role of the RAC1-WAVE-Arp2/3 pathway in sustaining migration in a direction chosen at random by single MCF10A cells (Molinie et al., 2019; Polesskaya et al., 2022). The human MCF10A cell line is derived from a fibrosis of mammary breast (Soule et al., 1990). Cells are diploid and not transformed, since they do not form tumors when grafted into immunocompromised mice (Worsham et al., 2005). These epithelial cells are quite plastic, as single cells detach from epithelial islets in vitro and adhere again to other cells when they meet. Arpin, ARPC1A and CYFIP2 play negative roles towards the polymerization of

cortical branched actin (CBA) at different levels of the RAC1-WAVE-Arp2/3 pathway (Fig.1A) and were inactivated.

To generate KO clones for each of these CBA negative regulators, we have created insertions/deletions (indels) in the Open Reading Frame (ORF) by transfecting synthetic gRNAs with the purified Cas9 protein into MCF10A cell line. In this protocol with no antibiotic selection, screening of about hundred clones by Western blot allowed to isolate at least two independent KO clones for each of these genes (Molinie et al., 2019; Polesskaya et al., 2022). We analyzed genomic DNA of these clones to characterize the indels. Genomic DNA encompassing the Cas9-mediated cut was amplified and the PCR product was sequenced. The PCR sequence could be directly read if the two alleles were the same. This was the case of ARPIN KO clone #1. If the PCR sequence cannot be read, it indicates that the two alleles generate different sequences that overlap. In this case, the PCR product was cloned and individual plasmids were then sequenced to unambiguously determine the sequence of the two alleles. In all clones, we were able to identify the indels that accounted for the 2 KO alleles due to frameshift (Fig.S1). For each of these CBA negative regulators, the two KO clones had increased migration persistence, although to a different extent (Fig.S2). This systematic increase of migration persistence was not associated with consistent variations of cell speed or Mean Square Displacement (MSD; Fig.S2), as we previously reported for MCF10A cells when the RAC1-WAVE-Arp2/3 pathway was perturbed (Molinie et al., 2019; Polesskaya et al., 2022).

To explore the potential synergistic role of regulatory proteins, we combined their KOs. Our goal was to see whether we could isolate a “super-migrator” cell line, since our protocol of gene inactivation, which does not require antibiotic selection, allows to perform the whole procedure again in a previously obtained KO cell line. For each CBA negative regulator, we edited further the KO clone that displayed the most increased migration persistence. We managed to obtain the 3 possible double KOs, ARPIN ARPC1A, ARPIN CYFIP2 and ARPC1A CYFIP2 (Fig.1B). To our surprise, none of the double KOs migrated more persistently than single KOs (Fig.1CD, Fig.S3). We thus attempted to combine the 3 KOs and this time, we obtained a super-migrator cell line that migrated more persistently than any single or double KO of ARPIN, CYFIP2, and ARPC1A (Fig.1CD, Movie S1).

To characterize the triple KO cells we had isolated, we first examined lamellipodia in fixed cells by immunofluorescence using phalloidin staining and an antibody targeting cortactin, a branched actin marker. MCF10A cells do not form prominent lamellipodia (Molinie et al., 2019). Staining of lamellipodia in triple KO cells was not different, with little enrichment of cortactin (Fig.2A). We thus decided to examine lamellipodial dynamics. Kymographs extracted from phase contrast imaging revealed that the rate of membrane protrusion, but not retraction, was significantly enhanced in triple KO compared with parental cells (Fig.2B,C). Upon transfection of cells with mCherry actin and TIRF-SIM imaging, we were able to image actin dynamics in lamellipodia (Fig.2D, Movie S2). As expected, we found that the actin polymerization rate at the lamllipodium edge, i.e. the sum of retrograde flow with membrane protrusion, was significantly enhanced in triple KO cells when compared with parental cells (Fig.2E).

A difficulty associated with this approach is that we could not afford to systematically study two independent clones for combined KOs, even though we had observed significant differences between single KO clones. This rule of keeping two independent clones for each genotype would mean 4 clones for each of the 3 double KOs and 8 clones for the triple KO. Moreover, if a clone adapts to its genotype, then the route taken to sequentially introduce mutations might potentially also affect the phenotype. In other words, the sequence by which compound KO were obtained might also influence the phenotype. To test all possible routes would double the number of double KO clones and multiply by 6 the number of triple KO clones. To be fully rigorous, the total number of clones to compare with parental cells would amount to 4x2 + 4x2 + 8x6 = 64 clones. This large number of clones prompted us to compare the super-migrator cell line we had obtained to the transient depletion of the 3 CBA negative regulators.

Knocking-down the 3 CBA negative regulators reveals a super-migrator phenotype in cell culture and zebrafish embryos

We transiently transfected MCF10A cells with pools of siRNAs targeting each of the 3 CBA negative regulators (Fig.3A). Upon siRNA-mediated depletion, double Knock-Down (KD) cells had the same increased migration persistence as single KD cells (Fig.3B; Fig.S4). Only the triple KD had increased persistence compared with all single or double KDs. The phenotype of the triple KD is thus most similar to the triple KO clone we isolated. A difference between the two approaches is that triple KD cells did not exhibit the slight increase of cell speed, previously seen in triple KO cells (Fig.3C). Together these experiments showed that MCF10A cells greatly increased migration persistence upon down-regulation of three, but not two CBA negative regulators, whether this down-regulation was performed by KO or KD.

To evaluate the physiological relevance of these observations, we turned to zebrafish embryos. We have previously characterized the migration of endodermal cells, which internalize at the beginning of gastrulation and then disperse over the yolk surface as single cells through random walks (Pézeron et al., 2008). This cell-autonomous migration process is governed by the Rac1 – Arp2/3 pathway (Giger and David, 2017; Woo et al., 2012). Using morpholinos, we knocked down Arpin, ARPC1A and CYFIP2 in endodermal cells and transplanted some into wild type receiver zebrafish embryos (Fig.4A, Fig.S5). Transplanted cells were tracked thanks to the expression of a Histone2B-mCherry fusion (Fig.4B, Movie S3).

When CBA negative regulators were tested in isolation, KD of CYFIP2 or Arpin significantly increased migration persistence of endodermal cells (Fig.4C), as we previously reported in the collective migration of prechordal plate cells (Dang et al., 2013; Polesskaya et al., 2022). Double KDs of Arpin and CYFIP2 led to an even stronger increase in persistence. ARPC1A KD had no effect on the migration of endodermal cells. Consistently, KDs of ARPC1A and CYFIP2 together led to a phenotype similar to simple CYFIP2 KD. But KDs of ARPC1A and Arpin increased cell persistence compared with the single KD of Arpin, as if ARPC1A potentiated the effect of Arpin. The triple depletion of Arpin, ARPC1A and CYFIP2 rendered cells significantly more persistent than all single or double depletions (Fig.4C, Fig.S5). Triple KD cells were also faster than other cells (Fig.4D). In conclusion, results observed in the zebrafish embryo largely mirror those obtained on MCF10A cells in culture, suggesting that KDs of the 3 CBA negative regulators turn cells into super-migrators in vivo as well as in culture cells.

The population of super-migrator triple KO cells is heterogeneous

We then asked whether promoting actin assembly and turning on migration persistence would be associated with defects. We thus decided to challenge our MCF10A KO clones into a morphogenetic assay, where single mammary cells proliferate and develop acini at the surface of matrigel (Debnath et al., 2003). We have previously reported that Arpin KO formed normal acini, albeit bigger than parental cells due to increased proliferation (Molinie et al., 2019). This was also the case upon KO of ARPC1A or CYFIP2 (Fig.5A,B). Acinus sizes reached by double KOs were not different from the ones of single KOs, but the biggest acini from triple KO reached a size bigger than the ones differentiated from single and double KOs. Parametric statistics could not be applied, because the size distribution of acini differentiated by the triple KO became scattered, with coexistence of small and large acini. Most large acini from the triple KO developed a lumen, more frequently so than the acini differentiated from parental cells (Fig.5C,D). Most small acini of the triple KO did not develop a lumen, in line with a delayed morphogenesis. Some of these small acini, however, displayed an irregular shape together with heterogeneous laminin deposition (Fig.5C). In conclusion, excessive activation of the Rac1-WAVE-Arp2/3 pathway did not only increase cell proliferation, as previously reported (Molinie et al., 2019), but also increased the heterogeneity of the cell population.

We then sought to analyze the triple KO for collective cell migration in a wound healing assay to examine how cells would coordinate with each other during cell migration, since Rac1-dependent polymerization of branched actin is critical both for lamellipodial protrusions at the front edge and for the maintenance of adherens junctions (Fenteany et al., 2000; Verma et al., 2004; Verma et al., 2012). The triple KO line that was super-migrating at the single cell level, did not improve wound healing, and even slightly decreased it, if anything (Fig.6A,B). The migrating front of the triple KO, however, appeared different from the one of parental cells (Movie S4). MCF10A cells closed the wound with a front that homogeneously progresses, unlike MDCK cells that organize multicellular 'fingers' pulled by leader cells (Poujade et al., 2007). The triple KO in MCF10A cells appeared more similar to MDCK cells than parental MCF10A cells, with protruding

fingers at the front. To quantify this effect, we measured the distance covered by the front over time. Overall, the mean value was quite similar between parental and triple KO cells, however, the variance was higher in triple KO than in parental cells due to these fingers at the leading front (Fig.6C).

We then decided to examine whether KO of CBA negative regulators would affect gene expression. We first analyzed all the genes of the Rac1-WAVE-Arp2/3 pathway in all KO cell lines that we had isolated for potential compensatory changes in gene expression. We found that, in line with non-sense mRNA mediated decay due to premature stop codons (Popp and Maquat, 2016), the levels of *CYFIP2, ARPIN* and *ARPC1A* mRNAs were greatly decreased when they contained indels in KO cell lines (Fig.S6). Down-regulation of CYFIP2 and ARPC1A was not compensated by transcriptional up-regulation of the paralogous genes, CYFIP1 and ARPC1B. Expression of genes encoding subunits of WAVE and Arp2/3 complexes was overall not significantly altered in KO cell lines, nor was the expression of genes encoding Rac small GTPases (Fig.S6, Table S1).

Because of the differential phenotype of the triple KO between single cell and collective migration, we also measured a set of 9 EMT genes, *VIM*, *CDH1*, CDH2, *SNAI1*, *SNAI2*, *TWIST1*, *ZO1*, *ZEB1* and *ZEB2*. Among EMT-related genes, we found that the expression of vimentin and of the transcription regulator ZEB2 were strongly down-regulated in all KOs, including single KOs (Fig.6D, Fig.S6). ZEB2 controls expression of the vimentin gene in MCF10A cells (Bindels et al., 2006). Down-regulation of vimentin gene expression translated into strongly decreased protein levels in all KO clones, but this effect was not observed upon transient KD of CBA inhibitors (Fig.6E). These results on selected genes showed that CBA can have an impact on gene expression. We thus performed RNAseq on all KO cell lines to study the global impact of CBA inhibitors (Table S2). 787 differentially expressed genes with an adjusted p-value inferior to 0.01 were identified between super-migrator triple KO and parental cells. Gene Ontology analysis revealed that most differentially expressed genes belonged to the category of genes involved in “cellular component organization or biogenesis”, encoding “cytosolic proteins” involved in “protein binding” (Table S3). The most strongly up-regulated gene in TKO cells was indeed *BEX3*, which encodes a signaling adaptor protein fulfilling these criteria. The most

strongly down-regulated one was *GPAT2* that encodes a mitochondrial glycerol 3-phosphate acyltransferase. Importantly, these two genes were respectively up- or down-regulated in all single KO, indicating that their expression was sensitive to the amount of CBA (Fig.S6).

When we examined vimentin expression and organization by immunofluorescence (Fig.6F), we found that vimentin was organized in a dense network in the majority of parental MCF10A cells. In contrast, single and double KOs had a decreased percentage of cells displaying such a network of vimentin filaments, and the triple KO even more so (Fig.6G). In wound healing assay, there was no absolute association between the leader cell phenotype and vimentin expression (Fig.6H). However, actively migrating leader cells in fingers were more likely to display a vimentin network than follower cells (Fig.6I).

Vimentin opposes migration persistence of single cells

We wondered if vimentin down-regulation in KO cell lines was promoting or opposing the increased migration persistence of these lines. We first examined the role of vimentin in parental MCF10A cells using two independent siRNAs (Fig.7A). Vimentin depletion dramatically increased migration persistence of single cells (Fig.7B, Fig.S7, Movie S5). Overexpression of untagged vimentin, however, did not yield any phenotype on persistence or other migration parameters of single cells (Fig.S7). In collective migration, vimentin-depleted MCF10A cells were less efficient at migrating than control cells, since they took longer to close the wound (Fig.7C). Similar to triple KO cells, single vimentin depleted cells displayed an increased rate of membrane protrusion, but not retraction (Fig.7D). Unlike triple KO cells, however, membrane protrusions of single vimentin depleted cells covered a wider distance, but lasted for shorter than the ones of parental cells. Therefore, the profound down-regulation of vimentin in triple KO cells might contribute to their exceptional migration persistence. To make this point, we isolated stable vimentin expressing cells from the triple KO super-migrating clone (Fig.7E). As expected, these clones displayed a higher proportion of cells with vimentin networks than triple KO population (Fig.7F). Most importantly, migration persistence of these cells was efficiently rescued, albeit not completely (Fig.7G, Fig.S8). These results suggest that the transcriptional

down-regulation of vimentin in super-migrating cells contributes to their migration persistence (Fig.8).

DISCUSSION

In this work, we combined the inactivation of 3 genes that antagonize migration persistence in MCF10A cells. In both KD and KO, there was no further effect when two genes were inactivated compared with a single inactivation, as if the system was buffered against a too dramatically enhanced persistence. Surprisingly, the addition of the third inactivation revealed dramatically enhanced persistence in the generated cells that we therefore referred to as super-migrators, as if the third inactivation enabled a threshold to be exceeded. This enhanced persistence of cell migration was presumably due to the enhanced actin polymerization rate we observed at membrane protrusions of triple KO cells together with their enhanced protrusion rate.

In zebrafish embryos, when we examined endodermal cells during gastrulation, the phenotype was roughly the same, since the triple inactivation generated cells that migrated more than any single or double KD. In the zebrafish system, however, an additional complexity was that the single ARPC1A KD did not generate a phenotype on its own, but amplified the persistence when combined with other KDs. Even if our super-migrators are very persistent, they are not yet similar to fish keratocytes, which are the most persistent vertebrate cells. To obtain the persistence and the characteristic morphology of fish keratocytes, it is perhaps required to combine our triple KO with inactivation of other negative regulatory genes. Among possible candidates, there are the Nance-Horan Syndrome protein NHSL1 (Law et al., 2021) and the Rac1 competitor CYRI (Fort et al., 2018).

The super-migrator phenotype of MCF10A cells was obtained with both triple KD and triple KO, but the mechanisms are different, because we identified down-regulation of vimentin with long-term inactivation in triple KO, but not in triple KD cells. Expression analyses showed that down-regulation of the genes encoding GPAT2, ZEB2 and vimentin was observed in all single KO indicating that it is a likely cell response to enhanced branched actin at the cortex. ZEB2 is a transcription factor the Zn finger family that was shown to control vimentin expression in MCF10A cells (Bindels et al., 2006). MCF10A cells are plastic epithelial cells, where cells in islets coexist with single cells, in regular culture conditions containing EGF. EGF induces

vimentin expression in MCF10A cells (Bindels et al., 2006). We found that vimentin down-regulation was to a large extent responsible for the persistence of triple KO, even though this mechanism was not at play in the super-migrators obtained upon triple KD. In line with our observation, vimentin intermediate filaments were previously reported to antagonize the actin retrograde flow from membrane protrusions (Costigliola et al., 2017) and disassembly of vimentin filaments was required to induce membrane protrusions by Rac1 signaling (Helfand et al., 2011).

The down-regulation of the EMT genes, ZEB2 and vimentin, in super-migrators indicates that cells respond to enhanced cortical branched actin by becoming more epithelial and less mesenchymal. The role of vimentin in fibroblasts is very distinct from the role we uncover here in epithelial cells. Vimentin KO mouse embryonic fibroblasts were found to be less motile in vitro and in vivo upon wound healing (Eckes et al., 1998; Eckes et al., 2000). Unlike MCF10A cells, rat fibroblasts were less directionally persistent when vimentin was KO (Vakhrusheva et al., 2019). These opposite roles of vimentin in the persistence of fibroblasts and epithelial cells are striking. Along this line, it is interesting to note that the persistent fish keratocytes are also single cells dissociated from an epithelial monolayer (Rapanan et al., 2014), as if the transcriptional program of epithelial cells render cells more persistent than fibroblasts when these epithelial cells happen to be isolated.

Super-migrator cells appeared less fit in collective behaviors than parental cells. Wound healing was less smooth with the apparition of leader cells at the front edge. Acinus morphogenesis was also affected. The triple KO cells differentiated into large acinus structures, as expected given the role of cortical branched actin in controlling cell cycle progression, but also into small acinus structures, which were abnormal in shape and extracellular matrix deposition. Importantly, despite their increased migration persistence as single cells, there was no sign of invasiveness, in line with the fact that these cells were driven towards a more epithelial program. Heterogeneity of the triple KO population was most evident at the level of vimentin expression and organization. Populations of cancer cells and aging cells are usually more heterogenous than populations of normal cells (Caspersson et al., 1963; Mahmoudi et al., 2019). Our work thus reveals that overactivation of the signaling pathway polymerizing cortical

branched actin alters gene expression programs in a variable manner in the different cells of the population and renders epithelial cells less able to coordinate in collective behaviors.

MATERIALS AND METHODS

Cells and Transfections

The MCF10A cell line was from the collection of breast cell lines organised by Thierry Dubois (Institut Curie, Paris), where they were authenticated. MCF10A cells were cultured in DMEM/F12 medium (Gibco) supplemented with 5% horse serum (Sigma), 100 ng/mL cholera toxin (Sigma), 20 ng/mL epidermal growth factor (Sigma), 0.01 mg/mL insulin (Sigma), 500 ng/mL hydrocortisone (Sigma) and 100 U/mL penicillin/streptomycin (Gibco). The MCF10A cell line and its derivatives were routinely tested for mycoplasma and found to be negative.

Human vimentin ORF (GenBank KU178388.1) was amplified from a vector provided by Dr. Alexander Minin (Institute of Protein Research of Russian Academy of Science). The PCR product was cloned into the home-made MXS CAG Blue SV40pA PGK Puro bGHpA between the FseI and AscI restriction sites and sequenced (Eurofins Genomics, Ebersberg, Germany) to ensure, that no mutations appeared after amplification. MCF10A cells were transfected using Lipofectamine 3000 (Invitrogen). Two days after transfection, 1 µg/mL Puromycin was added. Single clones were isolated by cloning rings, expanded and characterized.

For triple KD, cells were transfected using Lipofectamine RNAi max (Invitrogen) with 3 nM ARPC1A esiRNA (EHU105471, Sigma) (Molinie et al., 2019), 20 nM Arpin siRNA (5'-GUGGAUGUAUCUCGGCACA-3', onTarget Plus, Dharmacon) (Dang et al., 2013; Molinie et al., 2019; Simanov et al., 2021) and/or CYFIP2 (J-021477-05-0002, onTarget Plus, Dharmacon)(Polesskaya et al., 2022). Specific depletion was controlled with an equivalent amount of non-targeting siRNA (D-001810-01-05, onTarget Plus, Dharmacon) or GFP esiRNA (EHUEGFP, Sigma). siRNA-induced depletion of vimentin was obtained with 20 nM of siRNAs from Sigma, #1 5'-GUCUUGACCUUGAACGCAAdTdT-3', #2 – 5'-GGUUGAUACCCACUCAAAAdTdT-3' (Maier et al., 2015) and controlled with siCtrl–5'-AAUUCUCCGAACGUGUCACGUUU-3' (Fokin et al., 2021). Cells were harvested or imaged after two or three days.

Knock-out cell lines were generated using the CRISPR/Cas9 system. The following gRNAs were used: negative control 5'-AAAUGUGAGAUCAGAGUAAU-3'; *ARPIN* 5'-GAGAACUGAUCGAUGUAUCU-3'; *ARPC1A* 5'-UAAGAAGAACGGGAGCCAGU-3'; *CYFIP2* 5'-

CAUUUGUCACGGGCAUUGCA-3'. Cells were transfected with crRNA:tracrRNA duplex and the purified Cas9 protein by Lipofectamine CRISPRMAX™ Cas9 Transfection Reagent (all reagents were from Thermofisher Scientific). Cells then were subjected to dilution at 0.8 cells/well in 96 well plates. Clones were screened by Western blot. Targeted loci were amplified with the primers ARPINfor 5'-CCTGACAAGGTTCCTCCTGG-3', ARPINrev 5'-TGCTGCTCAACACAGCCTTA-3', ARPC1Afor 5'-ATTGACAGTTGTACGTGTCTCTG-3', ARPC1Arev 5'-AAAGGAAGAGTGCCTGATTTGGA-3', CYFIP2for 5'-GTTTCCACAGAGAGCTTGCG-3', CYFIP2rev 5'-GGAGCTCAAGAAAGTGAGTAGTG-3', and sequenced. In case of overlapping signals, PCR products were cloned (Zero Blunt PCR Cloning Kit, Thermofisher Scientific) and independent plasmids were sequenced to identify the 2 alleles.

Individual Migration of Endodermal Cells in Zebrafish Embryos

Embryos were obtained by natural spawning of Tg(-1.8gsc:GFP)ml1 adult fishes (Doitsidou et al., 2002). All animal studies were done in accordance with the guidelines issued by the Ministère de l'Education Nationale, de l'Enseignement Supérieur et de la Recherche and were approved by the Direction Départementale des Services Vétérinaires de l'Essonne and the Ethical Committee N°59.

Translation blocking morpholino (Gene Tool LLC Philomath) against ARPC1A (ATCTTCAAAGAATTTGCACCTCTGC) was designed for this study while morpholinos targeting CYFIP2 (CGACACAGGTTCACTCACAAAACAG) or Arpin (GTTGTCATAAATACGACTCATCTTC) were previously used and validated by rescue experiments in Dang et al., 2013; Polesskaya et al., 2021. To perform ARPC1A rescue experiments, morpholino insensitive mRNAs were synthesized from a pCS2+ plasmid containing the zebrafish coding sequence (Twist Bioscience), as the morpholino targets the 5' UTR.

Cells were forced to adopt an endodermal identity through the expression of the activated form of the Nodal receptor acvr1ba (acvr1ba*) (Peyriéras et al., 1998; Giger and David, 2017). Their nuclei were labeled through the expression of mCherry-tagged Histone2B.

All mRNAs were synthesized from pCS2+ plasmids with the mMessage mMachine SP6 kit (Thermo Fischer).

Donor embryos were injected at the 8-cell stage with 0.2 nl of a solution containing acvr1ba* (0.6 ng/µl), Histone2B-mCherry mRNA (30 ng/µl) and morpholinos against ARPC1A (0.2 mM), Arpin (0.2 mM) or CYFIP2 (0.2 mM), alone or in combination. Small groups of GFP expressing endodermal cells were transplanted at the shield stage (6 hpf) to the animal pole of an untreated host (Giger and David, 2017; Boutillon et al., 2018). Embryos were then cultured in embryo medium with 10 U/mL penicillin and 10 µg/mL streptomycin. Transplanted embryos were mounted in 0.2% agarose in embryo medium and imaged between shield stage and 85% epiboly (6 - 9 hpf) under an inverted TCS SP8 confocal microscope (Leica) equipped with environmental chamber (Life Imaging Services) at 28°C, using a HCX PL Fluotar 10x/0.3 objective (Leica). Visualization of 3D movies and nuclei tracking were done using Imaris (Bitplane). Cell migration parameters were extracted using custom codes in Matlab (Math Works) (Boutillon et al., 2022) and autocorrelation was computed using published Excel macros (Gorelik and Gautreau, 2014).

Antibodies

For Western blots, the following antibodies were used: CYFIP2 (Sigma SAB2701081, 1:1000), Tubulin clone DM1A (Sigma T9026, 1:2000), ARPC1A (Sigma #HPA004334, 1:200), Arpin home-made (Dang et al, 2013, 1:500), p62/DCTN4 clone H-4 (Santa Cruz Biotechnology, 1:200). For immunofluorescence anti-Laminin V, clone D4B5 (Merck, 1:100), anti-Cortactin, clone 4F11 (Merck, 1:200). For both applications, Anti-Vimentin, clone V9 (sc-6260, Santa Cruz, 1:100 for IF, 1:200 for WB) was used. Secondary goat anti-mouse and anti-rabbit antibodies conjugated with Alexa Fluor 488, 555 and 647 used for immunofluorescence at 1:300 dilution were from Life Technologies. Secondary goat anti-mouse and anti-rabbit antibodies conjugated with alkaline phosphatase used for Western blots (1:3000) were from Promega.

Western Blots

Cells were lysed in 50 mM Hepes, pH7.7, 150 mM NaCl, 1 mM CaCl2, 1% NP40, 0.5% Na Deoxycholate, and 0.1% SDS supplemented with a protease inhibitor cocktail (Roche). Lysates were spun at +4°C and 20000 xg and supernatants were mixed with LDS (ThermoFischer) and 2.5% of β-ME. SDS-PAGE was performed using NuPAGE 4–12% Bis-Tris gels (ThermoFischer Scientific). After transfer, nitrocellulose membranes were blocked in 5% skimmed milk incubated with primary and secondary antibodies conjugated with alkaline phosphatase and developed with NBT/BCIP as substrates (Promega). Uncropped Western blots are displayed in figure S9.

qRT-PCR & RNAseq

For qRT-PCR, total RNA was extracted from cell lines using the NucleoSpin RNA Plus Kit (Macherey-Nagel). Specific mRNAs were quantified from the cycle number (Ct value) at which the increase in the fluorescence signal started to be detected by the laser detector of the QuantStudio 7 Flex Real-Time PCR System (Thermo Fisher Scientific, Waltham, MA, USA) as previously described (Bieche et al., 2001). Gene expression levels were normalized to *TBP* expression levels (NM_003194) used as an endogenous RNA control and to the control condition, MCF10A parental cell line, to calculate the fold change. Nucleotide sequences of the primers used are detailed in Table S4.

For RNAseq, library was prepared using 150 ng of total RNA and QuantSeq 3' mRNA-Seq reverse (REV) Library Prep Kit (Lexogen, Vienna, Austria). The pool was sequenced on a NovaSeq 6000 SP 2x75bp flow cell (Illumina Inc., San Diego, CA). The raw sequencing data were deposited in the Gene Expression Omnibus (GEO) database under the accession number GSE244924. The BlueBee Genomics Plateform (Lexogen, Vienna, Austria) was used to generate normalized counts for each differential expression analysis. To identify genes whose expression was significantly misregulated an fold change > 1.5 for each KO cell line compared to Parental MCF10A cells was considered. To restrict the search to genes that were misregulated with a very high level of significance, the Padj-value threshold was set to the least Padj-value we found

for a knocked out gene. Analysis was carried out in R using the BiomaRt and ComplexHeatmap packages. Gene Ontology (GO) analysis of differentially expressed genes was carried out using g:Profiler website (https://biit.cs.ut.ee/gprofiler/gost). Table S3 reports molecular functions (GOMF), biological processes (GOBP), cellular components (GOCC) of differential expressed genes, as well as their mapping in pathways derived from KEGG (Kyoto Encyclopedia of Genes and Genomes) REAC (Reactome) and WP (WikiPathways) databases.

Live Cell Imaging

Videos of individual cell migration in 2D were acquired on an inverted Axio Observer microscope (Zeiss) equipped with a Pecon Zeiss incubator XL multi S1 RED LS (Heating Unit XL S, Temp module, CO2 module, Heating Insert PS and CO2 cover), a definite focus module and an ORCA-Flash4.0 V3 Digital CMOS camera. Pictures were taken every 5 or 10 min for 24 h using the Plan-Apochromat 20X/0.80 or Plan-Apochromat10X/0.40 air objectives. For wound healing, wounds were produced in a cell monolayer either by a pipet tip or by removing inserts from µ-dishes 35 mm (Ibidi). Cells were imaged every 20 minutes during 24 hours. For fast-acquisition of membrane dynamics, pictures were taken every 2 s for 5 min using the 63x/1.40 oil immersion objective.

For TIRF-SIM imaging, mCherry-actin transfected cells were plated onto glass-bottom dishes (Ibidi, 81158) that were coated with fibronectin. Images were acquired at 2 second intervals during 2 minutes using 3 phase shifted angles, each with 3 fringe patterns, on the Deltavision OMX SR (GE Healthcare) microscope. High resolution images were reconstructed in softWoRx (AppliedPrecision).

Acinus formation and staining

MCF10A cells were seeded on top of polymerized matrigel (CB-40230C, Corning) in Millicell EZ SLIDE 8-well glass chamber slide (PEZGS0816, Millipore) in a medium containing 4ng/mL EGF (4ng/mL) and 1% serum and supplemented with 2% of matrigel. During 3 weeks,

medium was regularly changed. Acini were then fixed in 2% PFA in PBS permeabilized with 0.5% Triton X-100, rinsed with PBS/glycine (130mM NaCl, 7mM Na2HPO4, 3.5mM NaH2PO4, 100mM glycine), blocked in IF Buffer (130mM NaCl, 7mM Na2HPO4, 3.5mM NaH2PO4, 0.1% bovine serum albumin, 0.2% Triton X-100, 0.05% Tween-20) + 10% FBS first and then with IF Buffer + 10% FBS + 20 µg/ml goat anti-Rabbit Fc fragment (111-005-046, Jackson ImmunoResearch). Acini were incubated with the primary antibodies in the secondary block solution washed with IF buffer and then incubated with secondary antibody in IF Buffer +10% FBS. Then acini were incubated with DAPI, rinsed with IF buffer and Mounted with Abberior Mount Liquid Antifade (Abberior) and sealed with nail polish. Overview images of acini were taken on an Olympus CKX53 microscope, equipped with a DP22 camera (Olympus) and DP2-SAL firmware (Olympus). Acinus size was then calculated in Fiji by manually contouring acini.

Immunofluorescence

Cells were seeded on glass coverslips coated with 20 µg/mL bovine fibronectin (Sigma) for 1 h at 37 °C. Cells were fixed in PBS/3.2% PFA then quenched with 50 mM NH_4Cl, permeabilised with 0.5 % Triton X-100, blocked in 2% BSA and incubated with antibodies (1-5 µg/mL for the primary, 5 µg/mL for the secondary) or 1:3000 diluted SiR-actin (Tebu-bio). Nuclei were counter stained with DAPI (Live Technologies). Images were acquired by Axio Observer microscope (Zeiss). Images of acini were obtained on a SP8ST-WS confocal microscope equipped with a HC PL APO 63x/1.40 oil immersion objective, a white light laser, HyD and PMT detectors.

Analysis of cell migration and lamellipodium dynamics

Image analysis was performed in ImageJ or FIJI software. In the single cell migration assay, only cells that were freely migrating for 7 h or more were taken into account. Cell trajectories were acquired with the ImageJ Manual tracking plugin. Random migration of single cells and migration persistence, based on the angular shift between frames, was analyzed as previously described (Dang et al., 2013) using the DiPer program (Gorelik and Gautreau, 2014).

To assess speed of wound closure, wound areas were manually drawn and measured at different time points. Variance of migration (St-Dev/Mean) in wound healing was calculated by measuring the distance moved by the leading edge perpendicular to the initial wound edge, for each pixel along the wound. To this end, time-lapse images were first thresholded, segmented in FIJI and analyzed using custom-made MATLAB scripts.

To analyse membrane dynamics, kymographs were obtained along a line that was perpendicular to the cell edge. Protrusion and retraction rates corresponding to protruding or retracting lamellipodia were extracted from the kymographs as tangents of angles. Protrusion length was measured manually. Duration of protrusion was defined as a total duration of observation (5 minutes) divided by the number of events. To analyse TIRF-SIM data, kymographs were generated in FIJI using manually drawn lines that followed the direction of actin retrograde flow. Protrusion/retraction speed and rearward flow were obtained as a tangent of the angle made with the time axis in kymographs. The actin assembly rate is the sum of protrusion speed and rearward flow.

Statistics

The autocorrelation curves corresponding to migration persistence were analyzed in R and fitted by an exponential decay, as described (Polesskaya et al., 2022)

$$A = (1 - A_{min}) * e^{-\frac{t}{\tau}} + A_{min}$$

where A is the autocorrelation, t the time interval, A_{min} the plateau, and τ the time constant of decay. The plateau value A_{min} is set to zero for the cell lines in vitro, as they do not display overall directional movement. Time constants τ, reflecting directional persistence, were then compared using one-way ANOVA on non-linear mixed-effect models to take into account the resampling of the same statistical unit. A minimum of 20 cells were analysed per condition to achieve sufficient statistical power. No data points were excluded from the analysis.

Other statistical analyses were carried out with GraphPad Prism software (v7.00) and Microsoft Excel 2016. When not stated otherwise, ANOVA and Kruskal-Wallis test were used. Shapiro-Wilk normality test was applied to examine whether data fit a normal distribution. If data satisfied the normality criterion, ANOVA was followed by a post-hoc Tukey's multiple comparison test. If not, a non-parametric Kruskal-Wallis test was followed by a post-hoc Dunn's multiple comparison test. Pairwise comparisons were assessed by either the t-test if data followed a normal distribution or by the Mann-Whitney test otherwise. 4 levels of significance were distinguished: * $p<0.05$, ** $p<0.01$, *** $p<0.001$, **** $p<0.0001$.

Author Contributions

AIF performed most experiments with human cells. YW contributed to the analysis of individual cell migration. JJ contributed to the analyses of collective cell migration and RNAseq data. GS and AP contributed to KO clone isolation and performed statistical analyses of migration persistence. AB and NBD performed cell migration experiments in Zebrafish. LC, SV and IB performed qRT-PCR and RNAseq experiments. NBD, IB and AMG performed supervision in their respective groups. AIF and AMG conceived the study, coordinated the work and wrote the manuscript.

Acknowledgements

We thank Dmitry Guschin and Pierre Mahou for excellent technical assistance, Alexander Minin for providing vimentin cDNA.

Funding

This work was supported by grants from Agence Nationale de la Recherche (ANR-20-CE13-0016 to AMG and NBD and ANR-22-CE13-0041 to AMG), Fondation ARC pour la Recherche sur le Cancer (ARC PJA 2021 060003815 to AMG), from Institut National du Cancer (INCA_11508 for AMG and IB, INCA_16712 for AMG). This work benefited from the support of the Personalized reconstitution of the tumoral process program led by l'X, Ecole polytechnique and the Fondation de l'Ecole polytechnique, sponsored by Servier. We thank the Polytechnique Bioimaging Facility for confocal microscopy partly supported by Région Ile-de-France (interDIM) and Agence Nationale de la Recherche (ANR-11-EQPX-0029 Morphoscope2, ANR-10-INBS-04 France BioImaging).

Conflict of Interest

The authors declare no conflict of interest.

Data Availability Statement

All data, plasmids and codes used in the study are available upon reasonable request. RNAseq data were deposited in the Gene Expression Omnibus (GEO) database under the accession number GSE244924.

REFERENCES

Abella, J. V. G., Galloni, C., Pernier, J., Barry, D. J., Kjær, S., Carlier, M.-F. and Way, M. (2016). Isoform diversity in the Arp2/3 complex determines actin filament dynamics. *Nature Cell Biology* **18**, 76–86.

Bieche, I., Parfait, B., Laurendeau, I., Girault, I., Vidaud, M. and Lidereau, R. (2001). Quantification of estrogen receptor alpha and beta expression in sporadic breast cancer. *Oncogene* **20**, 8109–8115.

Bieling, P. and Rottner, K. (2023). From WRC to Arp2/3: Collective molecular mechanisms of branched actin network assembly. *Curr Opin Cell Biol* **80**, 102156.

Bindels, S., Mestdagt, M., Vandewalle, C., Jacobs, N., Volders, L., Noël, A., Roy, F. van, Berx, G., Foidart, J.-M. and Gilles, C. (2006). Regulation of vimentin by SIP1 in human epithelial breast tumor cells. *Oncogene* **25**, 4975–4985.

Boutillon, A., Escot, S., Elouin, A., Jahn, D., González-Tirado, S., Starruß, J., Brusch, L. and David, N. B. (2022). Guidance by followers ensures long-range coordination of cell migration through α-catenin mechanoperception. *Dev Cell* **57**, 1529-1544.e5.

Caspersson, T., Foley, G. E., Killander, D. and Lomakka, G. (1963). Cytochemical differences between mammalian cell lines of normal and neoplastic origins Correlation with heterotransplantability in Syrian hamsters. *Exp Cell Res* **32**, 553–565.

Castro-Castro, A., Ojeda, V., Barreira, M., Sauzeau, V., Navarro-Lérida, I., Muriel, O., Couceiro, J. R., Pimentel-Muíños, F. X., Pozo, M. A. del and Bustelo, X. R. (2011). Coronin 1A promotes a cytoskeletal-based feedback loop that facilitates Rac1 translocation and activation. *The EMBO Journal* **30**, 3913–3927.

Chánez-Paredes, S., Montoya-García, A. and Schnoor, M. (2019). Cellular and pathophysiological consequences of Arp2/3 complex inhibition: role of inhibitory proteins and pharmacological compounds. *Cell Mol Life Sci* **76**, 3349–3361.

Costigliola, N., Ding, L., Burckhardt, C. J., Han, S. J., Gutierrez, E., Mota, A., Groisman, A., Mitchison, T. J. and Danuser, G. (2017). Vimentin fibers orient traction stress. *Proc. Natl. Acad. Sci.* **114**, 5195–5200.

Dang, I., Gorelik, R., Sousa-Blin, C., Derivery, E., Guérin, C., Linkner, J., Nemethova, M., Dumortier, J. G., Giger, F. A., Chipysheva, T. A., et al. (2013). Inhibitory signalling to the Arp2/3 complex steers cell migration. *Nature* **503**, 281–284.

Debnath, J., Muthuswamy, S. K. and Brugge, J. S. (2003). Morphogenesis and oncogenesis of MCF-10A mammary epithelial acini grown in three-dimensional basement membrane cultures. *Methods (San Diego, Calif.)* **30**, 256–268.

Ding, B., Yang, S., Schaks, M., Liu, Y., Brown, A. J., Rottner, K., Chowdhury, S. and Chen, B. (2022). Structures reveal a key mechanism of WAVE regulatory complex activation by Rac1 GTPase. *Nat Commun* **13**, 5444.

Eckes, B., Dogic, D., Colucci-Guyon, E., Wang, N., Maniotis, A., Ingber, D., Merckling, A., Langa, F., Aumailley, M., Delouvee, A., et al. (1998). Impaired mechanical stability, migration and contractile capacity in vimentin-deficient fibroblasts. *J Cell Sci* **111**, 1897–1907.

Eckes, B., Colucci-Guyon, E., Smola, H., Nodder, S., Babinet, C., Krieg, T. and Martin, P. (2000). Impaired wound healing in embryonic and adult mice lacking vimentin. *J Cell Sci* **113**, 2455–2462.

Fenteany, G., Janmey, P. A. and Stossel, T. P. (2000). Signaling pathways and cell mechanics involved in wound closure by epithelial cell sheets. *Curr Biol* **10**, 831–838.

Fokin, A. I., David, V., Oguievetskaia, K., Derivery, E., Stone, C. E., Cao, L., Rocques, N., Molinie, N., Henriot, V., Aumont-Nicaise, M., et al. (2021). The Arp1/11 minifilament of dynactin primes the endosomal Arp2/3 complex. *Sci Adv* **7**, eabd5956.

Fort, L., Batista, J. M., Thomason, P. A., Spence, H. J., Whitelaw, J. A., Tweedy, L., Greaves, J., Martin, K. J., Anderson, K. I., Brown, P., et al. (2018). Fam49/CYRI interacts with Rac1 and locally suppresses protrusions. *Nature Cell Biology* **20**, 1159–1171.

Fregoso, F. E., Eeuwen, T. van, Simanov, G., Rebowski, G., Boczkowska, M., Zimmet, A., Gautreau, A. M. and Dominguez, R. (2022). Molecular mechanism of Arp2/3 complex inhibition by Arpin. *Nat Commun* **13**, 628.

Giger, F. A. and David, N. B. (2017). Endodermal germ-layer formation through active actin-driven migration triggered by N-cadherin. *Proc National Acad Sci* **114**, 10143–10148.

Helfand, B. T., Mendez, M. G., Murthy, S. N. P., Shumaker, D. K., Grin, B., Mahammad, S., Aebi, U., Wedig, T., Wu, Y. I., Hahn, K. M., et al. (2011). Vimentin organization modulates the formation of lamellipodia. *Mol. Biol. Cell* **22**, 1274–1289.

Krause, M. and Gautreau, A. (2014). Steering cell migration: lamellipodium dynamics and the regulation of directional persistence. *Nature Reviews Mol Cell Biol* **15**, 577–590.

Law, A.-L., Jalal, S., Pallett, T., Mosis, F., Guni, A., Brayford, S., Yolland, L., Marcotti, S., Levitt, J. A., Poland, S. P., et al. (2021). Nance-Horan Syndrome-like 1 protein negatively regulates Scar/WAVE-Arp2/3 activity and inhibits lamellipodia stability and cell migration. *Nat Commun* **12**, 5687.

Li, J. X. H., Tang, V. W. and Brieher, W. M. (2020). Actin protrusions push at apical junctions to maintain E-cadherin adhesion. *Proceedings of the National Academy of Sciences of the United States of America* **117**, 432–438.

Mahmoudi, S., Mancini, E., Xu, L., Moore, A., Jahanbani, F., Hebestreit, K., Srinivasan, R., Li, X., Devarajan, K., Prélot, L., et al. (2019). Heterogeneity in old fibroblasts is linked to variability in reprogramming and wound healing. *Nature* **574**, 553–558.

Molinie, N. and Gautreau, A. (2018). The Arp2/3 Regulatory System and Its Deregulation in Cancer. *Physiological Reviews* **98**, 215–238.

Molinie, N., Rubtsova, S. N., Fokin, A., Visweshwaran, S. P., Rocques, N., Polesskaya, A., Schnitzler, A., Vacher, S., Denisov, E. V., Tashireva, L. A., et al. (2019). Cortical branched actin determines cell cycle progression. *Cell Research* **29**, 432–445.

Nieto, M. A., Huang, R. Y.-J., Jackson, R. A. and Thiery, J. P. (2016). EMT: 2016. *Cell* **166**, 21–45.

Palamidessi, A., Malinverno, C., Frittoli, E., Corallino, S., Barbieri, E., Sigismund, S., Beznoussenko, G. V., Martini, E., Garré, M., Ferrara, I., et al. (2019). Unjamming overcomes kinetic and proliferation arrest in terminally differentiated cells and promotes collective motility of carcinoma. *Nature materials* **80**, 076601.

Parrini, M. C., Sadou-Dubourgnoux, A., Aoki, K., Kunida, K., Biondini, M., Hatzoglou, A., Poullet, P., Formstecher, E., Yeaman, C., Matsuda, M., et al. (2011). SH3BP1, an exocyst-associated RhoGAP, inactivates Rac1 at the front to drive cell motility. *Molecular Cell* **42**, 650–661.

Paulin, D., Lilienbaum, A., Kardjian, S., Agbulut, O. and Li, Z. (2022). Vimentin: Regulation and pathogenesis. *Biochimie* **197**, 96–112.

Pézeron, G., Mourrain, P., Courty, S., Ghislain, J., Becker, T. S., Rosa, F. M. and David, N. B. (2008). Live Analysis of Endodermal Layer Formation Identifies Random Walk as a Novel Gastrulation Movement. *Current Biology* **18**, 276–281.

Polesskaya, A., Boutillon, A., Yang, S., Wang, Y., Romero, S., Liu, Y., Lavielle, M., Molinie, N., Rocques, N., Fokin, A., et al. (2022). Restrained activation of CYFIP2-containing WAVE complexes controls membrane protrusions and cell migration. *Biorxiv* 2020.07.02.184655.

Popp, M. W. and Maquat, L. E. (2016). Leveraging Rules of Nonsense-Mediated mRNA Decay for Genome Engineering and Personalized Medicine. *Cell* **165**, 1319–1322.

Poujade, M., Grasland-Mongrain, E., Hertzog, A., Jouanneau, J., Chavrier, P., Ladoux, B., Buguin, A. and Silberzan, P. (2007). Collective migration of an epithelial monolayer in response to a model wound. *Proceedings of the National Academy of Sciences* **104**, 15988–15993.

Puliafito, A., Hufnagel, L., Neveu, P., Streichan, S., Sigal, A., Fygenson, D. K. and Shraiman, B. I. (2012). Collective and single cell behavior in epithelial contact inhibition. *Proceedings of the National Academy of Sciences of the United States of America* **109**, 739–744.

Rapanan, J. L., Cooper, K. E., Leyva, K. J. and Hull, E. E. (2014). Collective cell migration of primary zebrafish keratocytes. *Exp Cell Res* **326**, 155–165.

Ridley, A. J. (2011). Life at the leading edge. *Cell* **145**, 1012–1022.

Rottner, K., Stradal, T. E. B. and Chen, B. (2021). WAVE regulatory complex. *Curr Biol* **31**, R512–R517.

Simanov, G., Dang, I., Fokin, A. I., Oguievetskaia, K., Campanacci, V., Cherfils, J. and Gautreau, A. M. (2021). Arpin Regulates Migration Persistence by Interacting with Both Tankyrases and the Arp2/3 Complex. *Int J Mol Sci* **22**, 4115.

Soule, H. D., Maloney, T. M., Wolman, S. R., Peterson, W. D., Brenz, R., McGrath, C. M., Russo, J., Pauley, R. J., Jones, R. F. and Brooks, S. C. (1990). Isolation and characterization of a spontaneously immortalized human breast epithelial cell line, MCF-10. *Cancer Research* **50**, 6075–6086.

Streichan, S. J., Hoerner, C. R., Schneidt, T., Holzer, D. and Hufnagel, L. (2014). Spatial constraints control cell proliferation in tissues. *Proceedings of the National Academy of Sciences* **111**, 5586–5591.

Thiery, J. P., Acloque, H., Huang, R. Y. J. and Nieto, M. A. (2009). Epithelial-Mesenchymal Transitions in Development and Disease. *Cell* **139**, 871–890.

Vakhrusheva, A., Endzhievskaya, S., Zhuikov, V., Nekrasova, T., Parshina, E., Ovsiannikova, N., Popov, V., Bagrov, D., Minin, A. A. and Sokolova, O. S. (2019). The role of vimentin in directional migration of rat fibroblasts. *Cytoskeleton* **76**, 467–476.

Verma, S., Shewan, A. M., Scott, J. A., Helwani, F. M., Elzen, N. R. den, Miki, H., Takenawa, T. and Yap, A. S. (2004). Arp2/3 activity is necessary for efficient formation of E-cadherin adhesive contacts. *The Journal of biological chemistry* **279**, 34062–34070.

Verma, S., Han, S. P., Michael, M., Gomez, G. A., Yang, Z., Teasdale, R. D., Ratheesh, A., Kovacs, E. M., Ali, R. G. and Yap, A. S. (2012). A WAVE2-Arp2/3 actin nucleator apparatus supports junctional tension at the epithelial zonula adherens. *Molecular Biology of the Cell* **23**, 4601–4610.

Wang, Y., Chiappetta, G., Guérois, R., Romero, S., Krause, M., Dessalles, C., Babataheri, A., Barakat, A. I., Vinh, J., Polesskaya, A., et al. (2022). PPP2R1A Regulates Migration Persistence through the WAVE Shell Complex. *Biorxiv* 2022.06.02.494622.

Woo, S., Housley, M. P., Weiner, O. D. and Stainier, D. Y. R. (2012). Nodal signaling regulates endodermal cell motility and actin dynamics via Rac1 and Prex1. *The Journal of Cell Biology* **198**, 941–952.

Worsham, M. J., Pals, G., Schouten, J. P., Miller, F., Tiwari, N., Spaendonk, R. van and Wolman, S. R. (2005). High-resolution mapping of molecular events associated with immortalization, transformation, and progression to breast cancer in the MCF10 model. *Breast Cancer Research and Treatment* **96**, 177–186.

Wu, C., Asokan, S. B., Berginski, M. E., Haynes, E. M., Sharpless, N. E., Griffith, J. D., Gomez, S. M. and Bear, J. E. (2012). Arp2/3 is critical for lamellipodia and response to extracellular matrix cues but is dispensable for chemotaxis. *Cell* **148**, 973–987.

Yamazaki, D., Itoh, T., Miki, H. and Takenawa, T. (2013). srGAP1 regulates lamellipodial dynamics and cell migratory behavior by modulating Rac1 activity. *Molecular Biology of the Cell* **24**, 3393–3405.

Yelland, T., Le, A. H., Nikolaou, S., Insall, R., Machesky, L. and Ismail, S. (2021). Structural Basis of CYRI-B Direct Competition with Scar/WAVE Complex for Rac1. *Structure* **29**, 226-237.e4.

Zhao, K., Wang, D., Zhao, X., Wang, C., Gao, Y., Liu, K., Wang, F., Wu, X., Wang, X., Sun, L., et al. (2020). WDR63 inhibits Arp2/3-dependent actin polymerization and mediates the function of p53 in suppressing metastasis. *Embo Rep* **21**, e49269.

Figure legends

Figure 1. Simultaneous KO of 3 CBA negative regulators increases migration persistence. (A) Scheme representing the role of each CBA negative regulator, Arpin, ARPC1A and CYFIP2 in the Rac1-WAVE-Arp2/3 pathway. (B) MCF10A cells were depleted of the 3 CBA negative regulators in various combinations using Cas9-mediated knock-out (KO). Western blots of target proteins. (C) Migration persistence of KO cells. Mean ± s.e.m. Curves are compared by ANOVA on non-linear mixed-effect models. (D) Average speed of KO cells. Mean ± s.d. Kruskal-Wallis test. Three independent experiments gave similar results. For graphical display, data were pooled for a total of n > 63. ANOVA, * p<0.05, ** p<0.01, **** p<0.0001.

Figure 2. Enhanced membrane dynamics in triple KO cells. (A) MCF10A parental and triple KO cells were stained with DAPI, phalloidin and antibodies to cortactin, a branched actin marker. Insets correspond to magnified parts of the leading edge. (B) Kymograph obtained along the white line of the still image. Scale bar: 10 µm. (C) Quantification. Three independent experiments gave similar results. For graphical display, data were pooled for a total of n=35. Mean ± s.d. Unpaired t test with Welch's correction, *** p<0.001, n.s. non-significant. (D) TIRF-SIM imaging of mCherry-actin. Kymograph obtained along the white line of the still image. Scale bar: 5 µm. (E) Quantification. The actin polymerization rate is the sum of protrusion rate and actin retrograde flow. Mean ± s.d. Two independent experiments gave similar results. For graphical display, data were pooled for a total of n=26. Mann-Whitney test, **** p<0.0001, n.s. non-significant.

Figure 3. Simultaneous KD of 3 CBA negative regulators increases migration persistence. (A) MCF10A cells were depleted of the 3 CBA negative regulators in various combinations using siRNAs. Western

blots. (B) Migration persistence of knock-down (KD) cells. Mean ± s.e.m. Curves were compared by ANOVA on non-linear mixed-effect models. (C) Average speed of KD cells. Mean ± s.d. Kruskal-Wallis test. Three independent experiments gave similar results. For graphical display, data were pooled for a total of n > 21. ANOVA, * p<0.05, ** p<0.01.

Figure 4. Enhanced migration of endodermal cells in Zebrafish embryos upon morpholino-mediated KD of CBA negative regulators. (A) Transplantation of Histone 2B-mCherry-labeled endodermal cells from a gsc:GFP transgenic donor embryo to a receiver embryo allows to monitor migration of single endodermal cells. (B) Dissemination of labeled cells over time. Scale bar: 50 µm. (C) Migration persistence of endodermal cells. Mean ± s.e.m. Curves are compared by ANOVA on non-linear mixed-effect models. (D) Average speed of endodermal cells per embryo. Mean ± s.e.m. Mann-Whitney test. Number of embryos/average number of cells in each embryo per condition: Ctrl 9/58, Arpin 9/32, ARPC1A 10/32, CYFIP2 20/39, ARPC1A+Arpin 10/23, CYFIP2+Arpin 9/58, CYFIP2 + ARPC1A 10/13, triple 16/14. An average of 33 cells were transplanted in each embryo. * p<0.05, ** p<0.01, *** p<0.001, **** p<0.0001, n.s. non-significant. When not otherwise indicated, p refers to the comparison with the WT condition.

Figure 5. Inactivation of CBA negative regulators alter acini morphogenesis. (A) Overview of MCF10A acini growing on top of matrigel. Scale bar: 200 µm. (B) Acini size. Apparent area (mean ± s.d.) is plotted. Bigger acini were formed when more CBA inhibitors were inactivated, but size heterogeneity also increases. (C) MCF10A acini derived from parental and triple KO cells were stained with DAPI and phalloidin to visualize nuclei and actin filaments and with laminin antibodies to reveal the extracellular matrix secreted by MCF10A acini. In triple KO, large acini often contained a single lumen, whereas small acini had no lumen. Small acini tend to deposit laminin irregularly and display irregular shapes. Scale bar: 50 µm. (D) Quantification. n = 26 acini for parental and n = 22 acini for triple KO.

Figure 6. Altered collective behaviors and heterogeneity of vimentin expression in MCF10A cells inactivated for CBA negative regulators. (A) Wound healing in triple KO and parental cells. Mean ± s.d. of 18 wounds (n=18, 3 fields of view per condition from 6 independent experiments). 2-way ANOVA, n.s. non-significant. (B) Heterogeneous behaviors of triple KO cells at the migration front. Fingers develop at

the edge of triple KO monolayers, but not of parental cell monolayers. Scale bar: 100 µm. (C) Quantification of edge fluctuations. The position of front cells is reported over time and compared to the initial position to calculate the distance traveled by front cells. The ratio of SD over mean of this value is calculated for multiple fields of view (n = 6) and plotted against time after wounding. Mann-Whitney test over areas under curve. (D) Relative levels of vimentin mRNA in KO cell lines. qPCR was performed in triplicates and normalized by the mRNA level of GAPDH. Fold change in each replicate is shown as individual data points and mean ± s.d. ANOVA, followed by the Dunnett's multiple comparisons test. (E) Vimentin is down-regulated upon KO of CBA negative regulators, but not KD. Western blots. (F) Parental and triple KO cells were stained with DAPI, phalloidin (actin), and vimentin antibodies. The population of triple KO cells is heterogeneous in vimentin organization. 3 categories of cells are distinguished in the triple KO population and illustrated by a magnified representative example. Scale bar: 20 µm. (G) Quantification. For each condition, more than 400 cells in 11 fields of view were pooled from 2 independent experiments. The two experiments gave similar results. Kruskal-Wallis test, * $p<0.05$, ** $p<0.01$, n.s. non-significant. (H) Parental and triple KO cells were stained with DAPI, phalloidin (actin), and vimentin antibodies, 7 h after wounding. In triple KO monolayers, leader cells labeled L in finger-like protrusions were distinguished from neighboring followers cells labeled F. (I) Quantification. 109 L and F cells from 3 independent wounds. Welch's unequal variance t-test, ** $p<0.01$.

Figure 7. Vimentin antagonizes migration persistence of single cells. (A) MCF10A cells were depleted of vimentin using siRNAs. Western blots. (B) Migration persistence of single cells. Two independent experiments gave similar results. For graphical display, data were pooled for a total of n = 60, mean ± s.e.m. Curves are compared by ANOVA on non-linear mixed-effect models. **** $p<0.0001$. (C) Wound healing. The dashed line indicates full closure. 10 wounds for each condition were analyzed. 2-way ANOVA, * $p<0.05$, **** $p<0.0001$. (D) Analysis of membrane dynamics upon vimentin depletion. Rates of membrane protrusion or retraction, as well as protrusion length and protrusion frequency are plotted. Three independent experiments gave similar results. For graphical display, data were pooled for a total of n=26. Mann-Whitney test, * $p<0.05$, **** $p<0.0001$, n.s. non-significant. (E) Western blots of parental, triple KO and triple KO transfected by a plasmid expressing untagged vimentin or by an empty plasmid as a control. A single Western blot, where intervening lanes have been removed, is shown for each antibody. (F) Quantification of the percentage of cells displaying different types of vimentin

organization. More than 400 cells per condition were taken into account. The category “no vimentin staining” is compared by Kruskal-Wallis test. *** $p<0.001$,**** $p<0.0001$, n.s. non-significant. (G) Migration persistence of single cells. Two independent experiments gave similar results. For graphical display, data were pooled for a total of $n > 65$. Curves are compared by ANOVA on non-linear mixed-effect models, ** $p<0.01$, **** $p<0.0001$.

Figure 8. Model. In control cells, multiple molecular machines activated by Rac1 polymerizes branched actin in membrane protrusions. Active machines, CYFIP1-containing WAVE complexes and ARPC1B-containing Arp2/3 complexes, are balanced by relatively less active machines such as CYFIP2-containing WAVE complexes and ARPC1A-containing Arp2/3 complexes and by the Arp2/3 inhibitory protein Arpin. This balance results in moderately persistent cells. In super-migrator cells, where CYFIP2, ARPC1A and Arpin are inactivated, membrane protrusions are sustained by enhanced cortical branched actin and persistence of cell migration increases. Continuous overactivation of cortical branched actin in triple KO, but not in triple KD results in down-regulation of vimentin expression, which contributes to enhanced migration persistence.

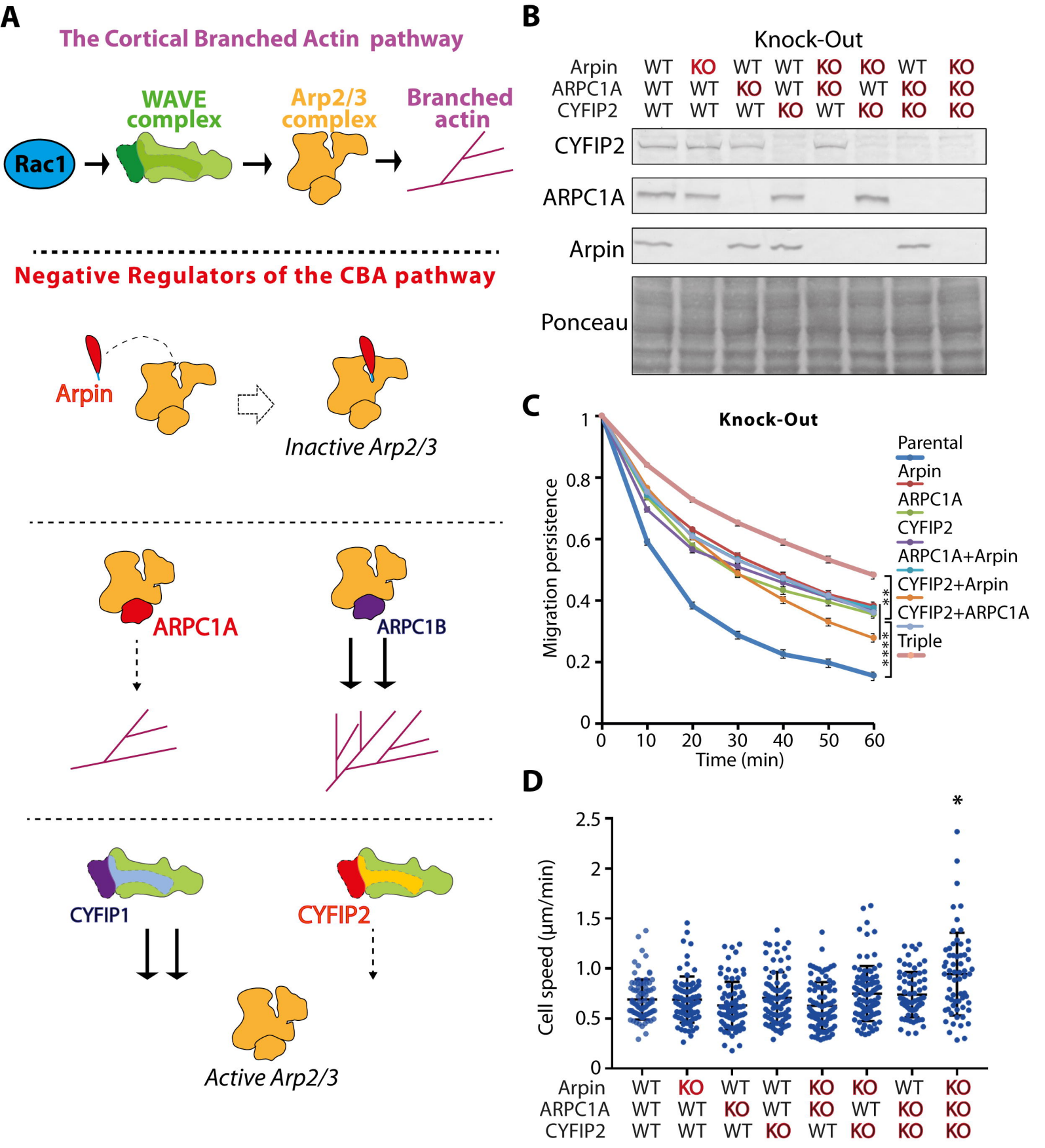
A
The Cortical Branched Actin pathway
Rac1
WAVE complex
Arp2/3 complex
Branched actin
Negative Regulators of the CBA pathway
Arpin
Inactive Arp2/3
ARPC1A
ARPC1B
CYFIP1
CYFIP2
Active Arp2/3
B
Knock-Out
Arpin WT KO WT WT KO KO WT KO
ARPC1A WT WT KO WT KO WT KO KO
CYFIP2 WT WT WT KO WT KO KO KO
CYFIP2
ARPC1A
Arpin
Ponceau
C
Knock-Out
Migration persistence
Time (min)
Parental
Arpin
ARPC1A
CYFIP2
ARPC1A+Arpin
CYFIP2+Arpin
CYFIP2+ARPC1A
Triple
D
Cell speed (µm/min)
Arpin WT KO WT WT KO KO WT KO
ARPC1A WT WT KO WT KO WT KO KO
CYFIP2 WT WT WT KO WT KO KO KO

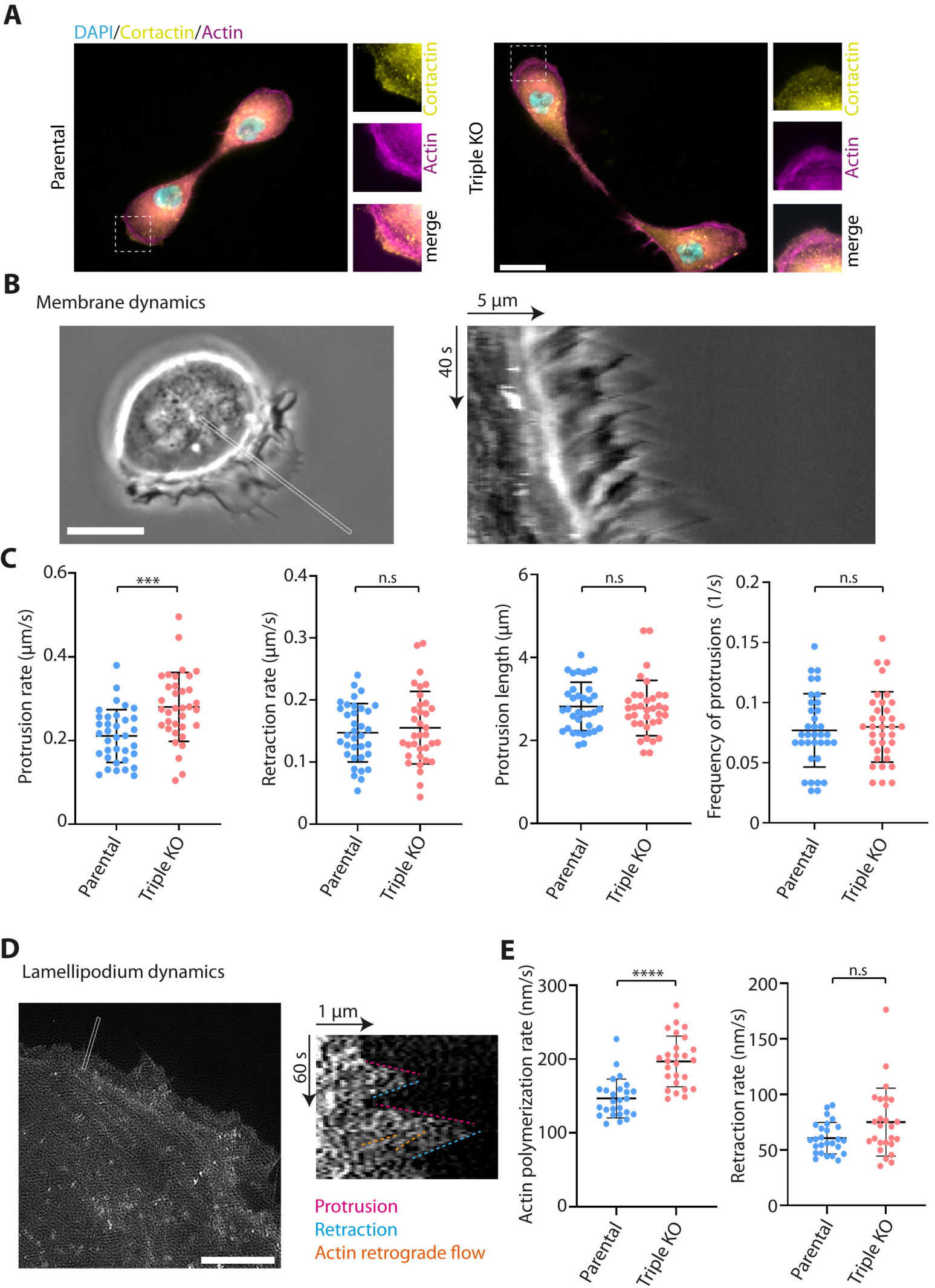
A
DAPI/Cortactin/Actin
Parental
Cortactin
Actin
merge
Triple KO
Cortactin
Actin
merge
B
Membrane dynamics
5 µm
40 s
C
Protrusion rate (µm/s)
0.6
0.4
0.2
0
***
Parental
Triple KO
Retraction rate (µm/s)
0.4
0.3
0.2
0.1
0
n.s
Parental
Triple KO
Protrusion length (µm)
6
4
2
0
n.s
Parental
Triple KO
Frequency of protrusions (1/s)
0.2
0.15
0.1
0.05
0
n.s
Parental
Triple KO
D
Lamellipodium dynamics
1 µm
60 s
Protrusion
Retraction
Actin retrograde flow
E
Actin polymerization rate (nm/s)
300
200
100
0
****
Parental
Triple KO
Retraction rate (nm/s)
200
150
100
50
0
n.s
Parental
Triple KO

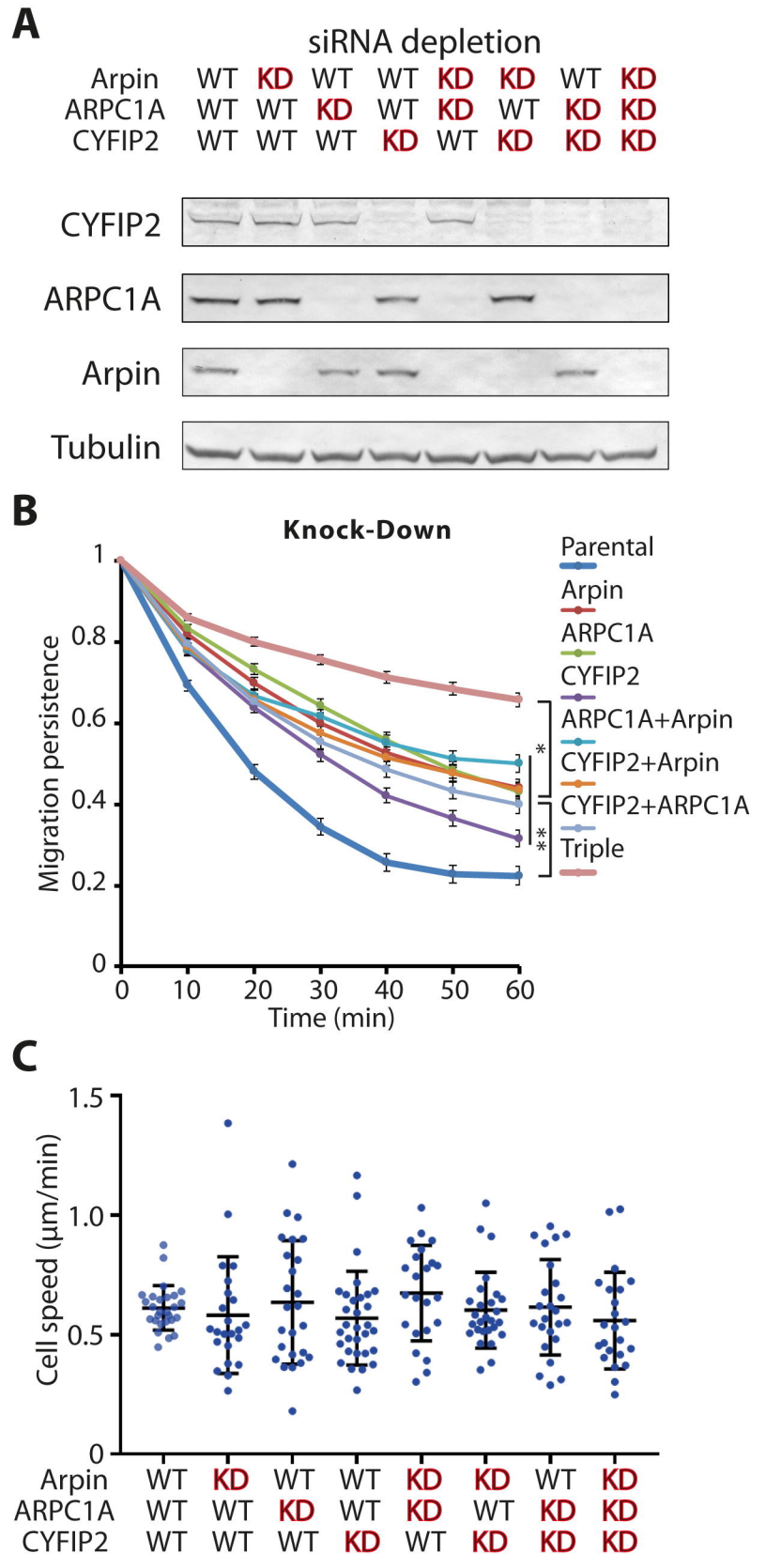
A
siRNA depletion
Arpin WT KD WT WT KD KD WT KD
ARPC1A WT WT KD WT KD WT KD KD
CYFIP2 WT WT WT KD WT KD KD KD
CYFIP2
ARPC1A
Arpin
Tubulin
B
Knock-Down
Migration persistence
Time (min)
Parental
Arpin
ARPC1A
CYFIP2
ARPC1A+Arpin
CYFIP2+Arpin
CYFIP2+ARPC1A
Triple
*
**
C
Cell speed (µm/min)
Arpin WT KD WT WT KD KD WT KD
ARPC1A WT WT KD WT KD WT KD KD
CYFIP2 WT WT WT KD WT KD KD KD

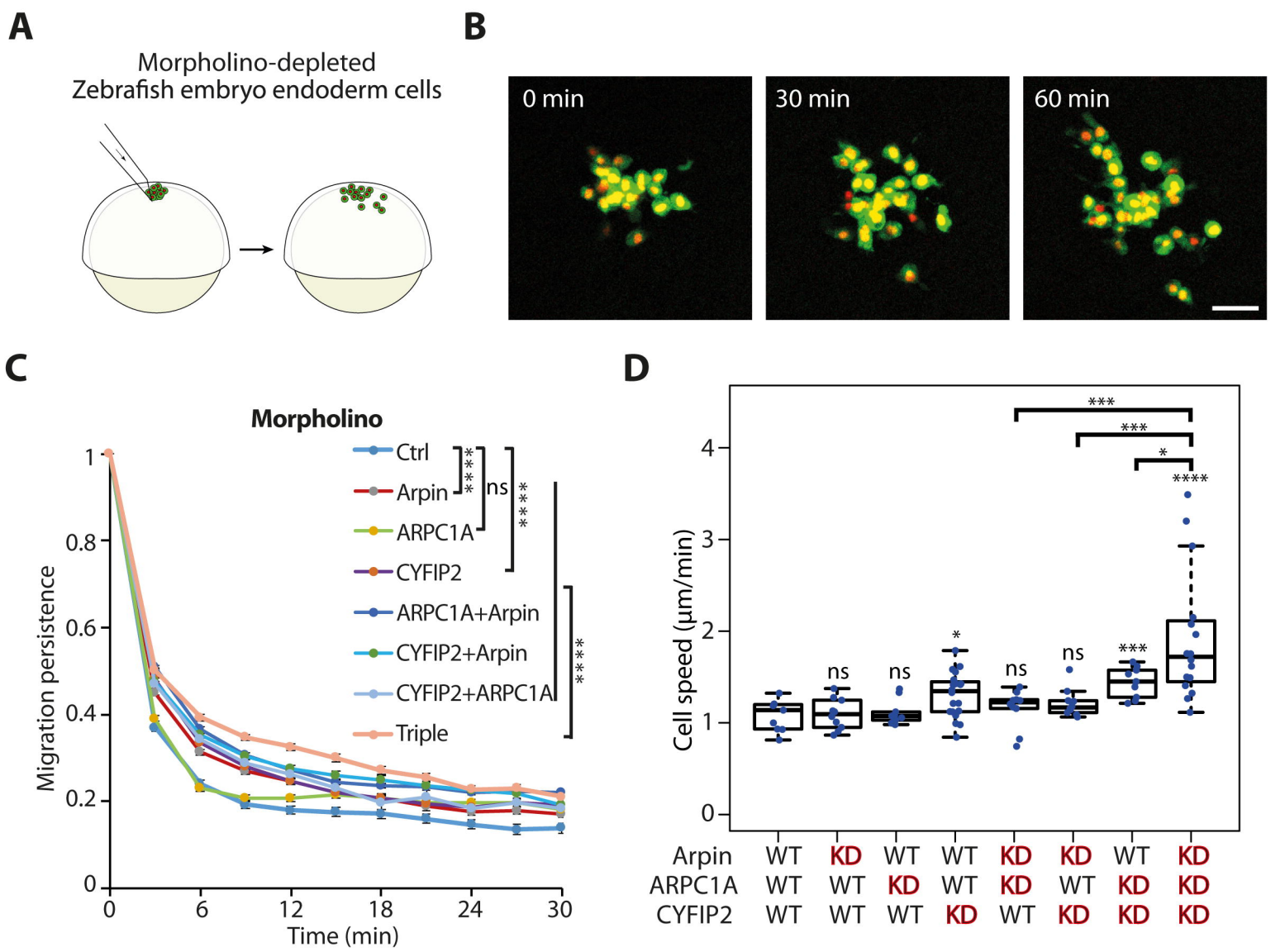
A
Morpholino-depleted
Zebrafish embryo endoderm cells
B
0 min
30 min
60 min
C
Morpholino
Ctrl
Arpin
ARPC1A
CYFIP2
ARPC1A+Arpin
CYFIP2+Arpin
CYFIP2+ARPC1A
Triple
****
ns
****
****
Migration persistence
Time (min)
D
Cell speed (µm/min)
***
***
*
****
ns
ns
*
ns
ns
***
Arpin WT KD WT WT KD KD WT KD
ARPC1A WT WT KD WT KD WT KD KD
CYFIP2 WT WT WT KD WT KD KD KD

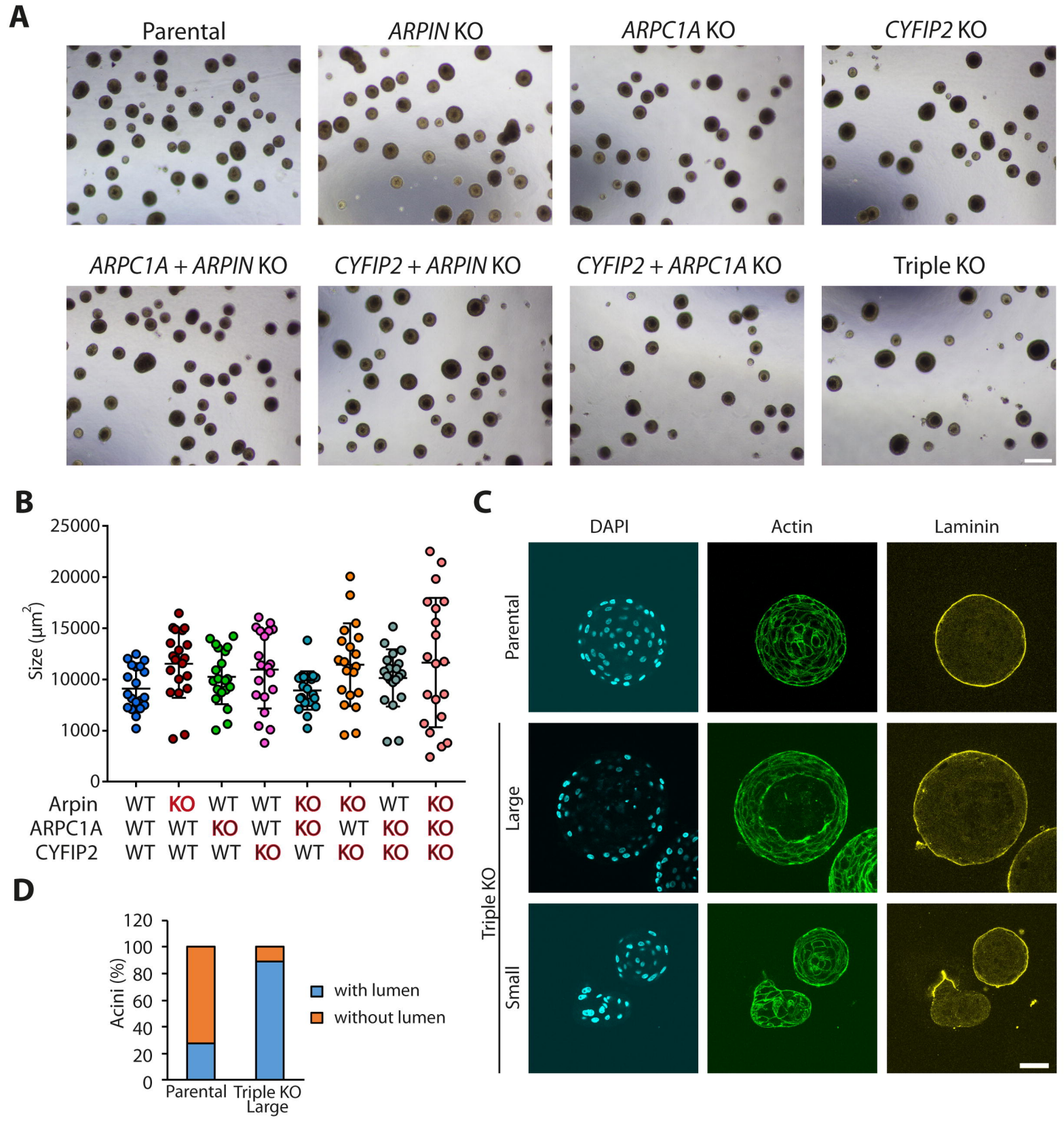
A
Parental
ARPIN KO
ARPC1A KO
CYFIP2 KO
ARPC1A + ARPIN KO
CYFIP2 + ARPIN KO
CYFIP2 + ARPC1A KO
Triple KO
B
Size (µm²)
25000
20000
15000
10000
1000
0
Arpin WT KO WT WT KO KO WT KO
ARPC1A WT WT KO WT KO WT KO KO
CYFIP2 WT WT WT KO WT KO KO KO
C
DAPI
Actin
Laminin
Parental
Triple KO
Large
Small
D
Acini (%)
120
100
80
60
40
20
0
Parental
Triple KO Large
with lumen
without lumen

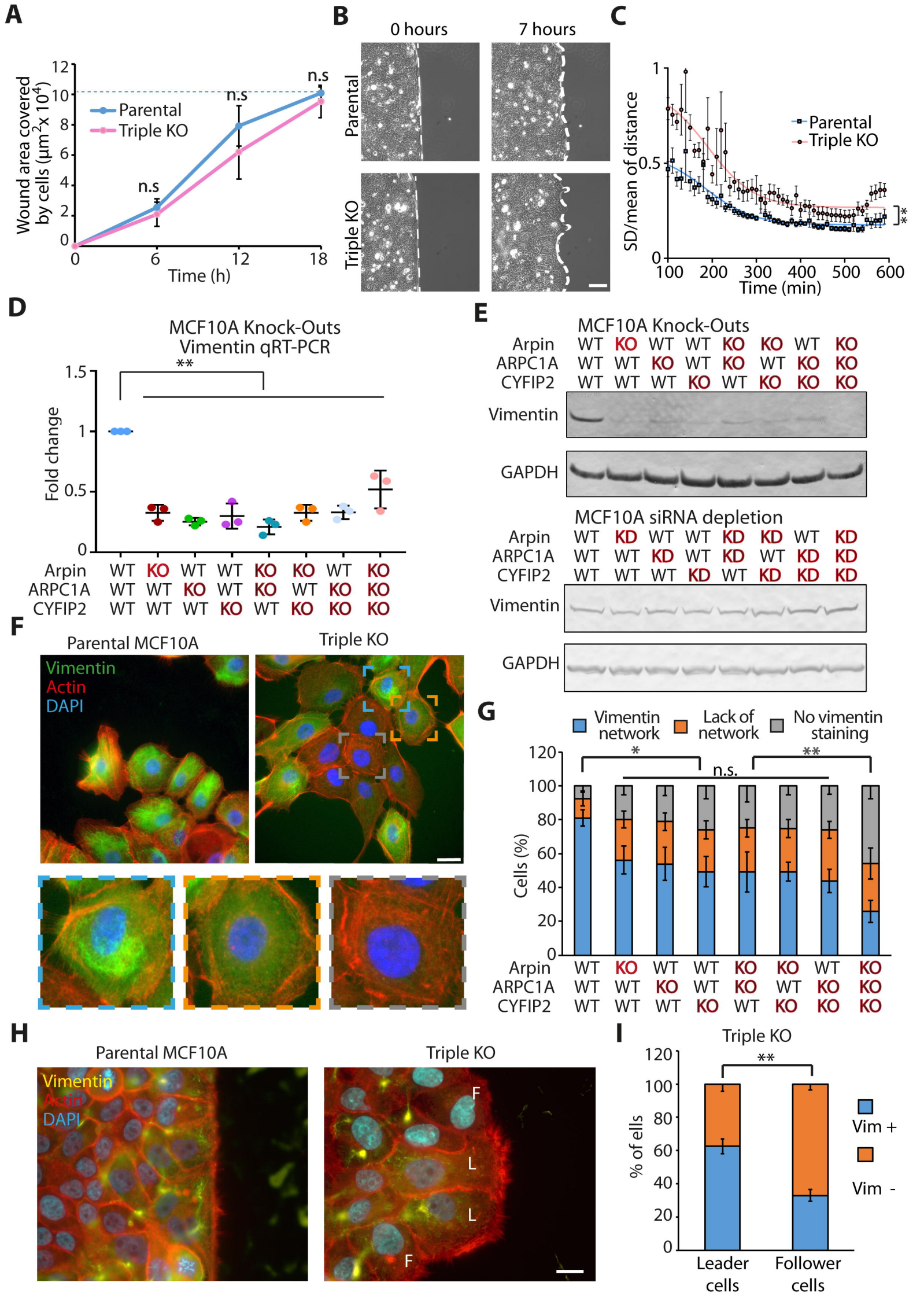
A
Wound area covered by cells (μm²x 10⁴)
Parental
Triple KO
n.s
n.s
n.s
Time (h)
B
0 hours
7 hours
Parental
Triple KO
C
SD/mean of distance
Parental
Triple KO
Time (min)
D
MCF10A Knock-Outs
Vimentin qRT-PCR
**
Fold change
Arpin WT KO WT WT KO KO WT KO
ARPC1A WT WT KO WT KO WT KO KO
CYFIP2 WT WT WT KO WT KO KO KO
E
MCF10A Knock-Outs
Arpin WT KO WT WT KO KO WT KO
ARPC1A WT WT KO WT KO WT KO KO
CYFIP2 WT WT WT KO WT KO KO KO
Vimentin
GAPDH
MCF10A siRNA depletion
Arpin WT KD WT WT KD KD WT KD
ARPC1A WT WT KD WT KD WT KD KD
CYFIP2 WT WT WT KD WT KD KD KD
Vimentin
GAPDH
F
Parental MCF10A
Triple KO
Vimentin
Actin
DAPI
G
Vimentin network
Lack of network
No vimentin staining
*
n.s.
**
Cells (%)
Arpin WT KO WT WT KO KO WT KO
ARPC1A WT WT KO WT KO WT KO KO
CYFIP2 WT WT WT KO WT KO KO KO
H
Parental MCF10A
Triple KO
Vimentin
Actin
DAPI
F
L
L
F
I
Triple KO
**
% of cells
Vim +
Vim -
Leader cells
Follower cells

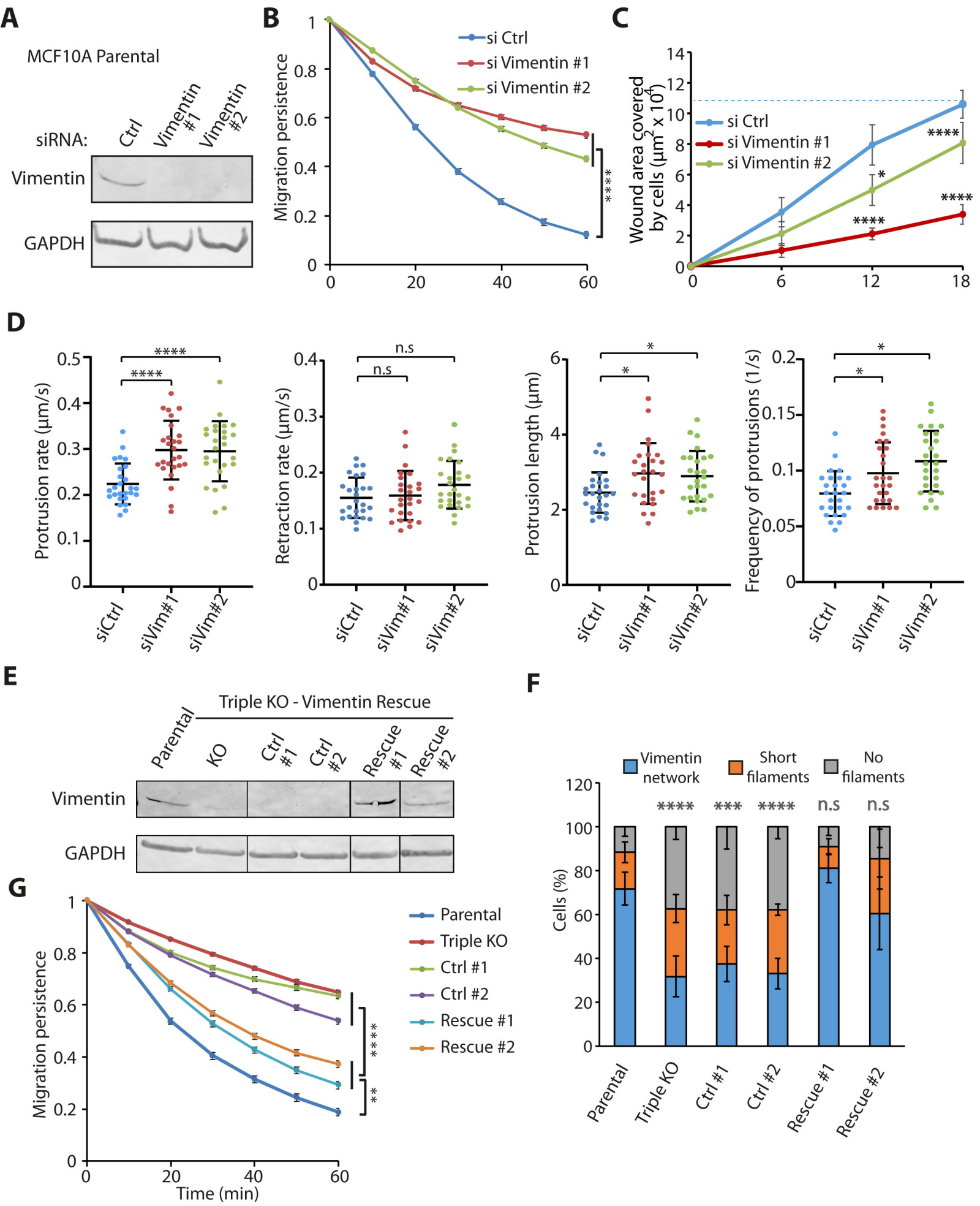
A
MCF10A Parental
siRNA:
Ctrl
Vimentin #1
Vimentin #2
Vimentin
GAPDH
B
Migration persistence
si Ctrl
si Vimentin #1
si Vimentin #2
****
C
Wound area covered by cells (μm² x 10⁴)
si Ctrl
si Vimentin #1
si Vimentin #2
****
*
****
****
D
Protrusion rate (μm/s)
****
****
Retraction rate (μm/s)
n.s
n.s
Protrusion length (μm)
*
*
Frequency of protrusions (1/s)
*
*
siCtrl
siVim#1
siVim#2
E
Triple KO - Vimentin Rescue
Parental
KO
Ctrl #1
Ctrl #2
Rescue #1
Rescue #2
Vimentin
GAPDH
F
Vimentin network
Short filaments
No filaments
Cells (%)
****
***
****
n.s
n.s
Parental
Triple KO
Ctrl #1
Ctrl #2
Rescue #1
Rescue #2
G
Migration persistence
Parental
Triple KO
Ctrl #1
Ctrl #2
Rescue #1
Rescue #2
****
****
**
Time (min)

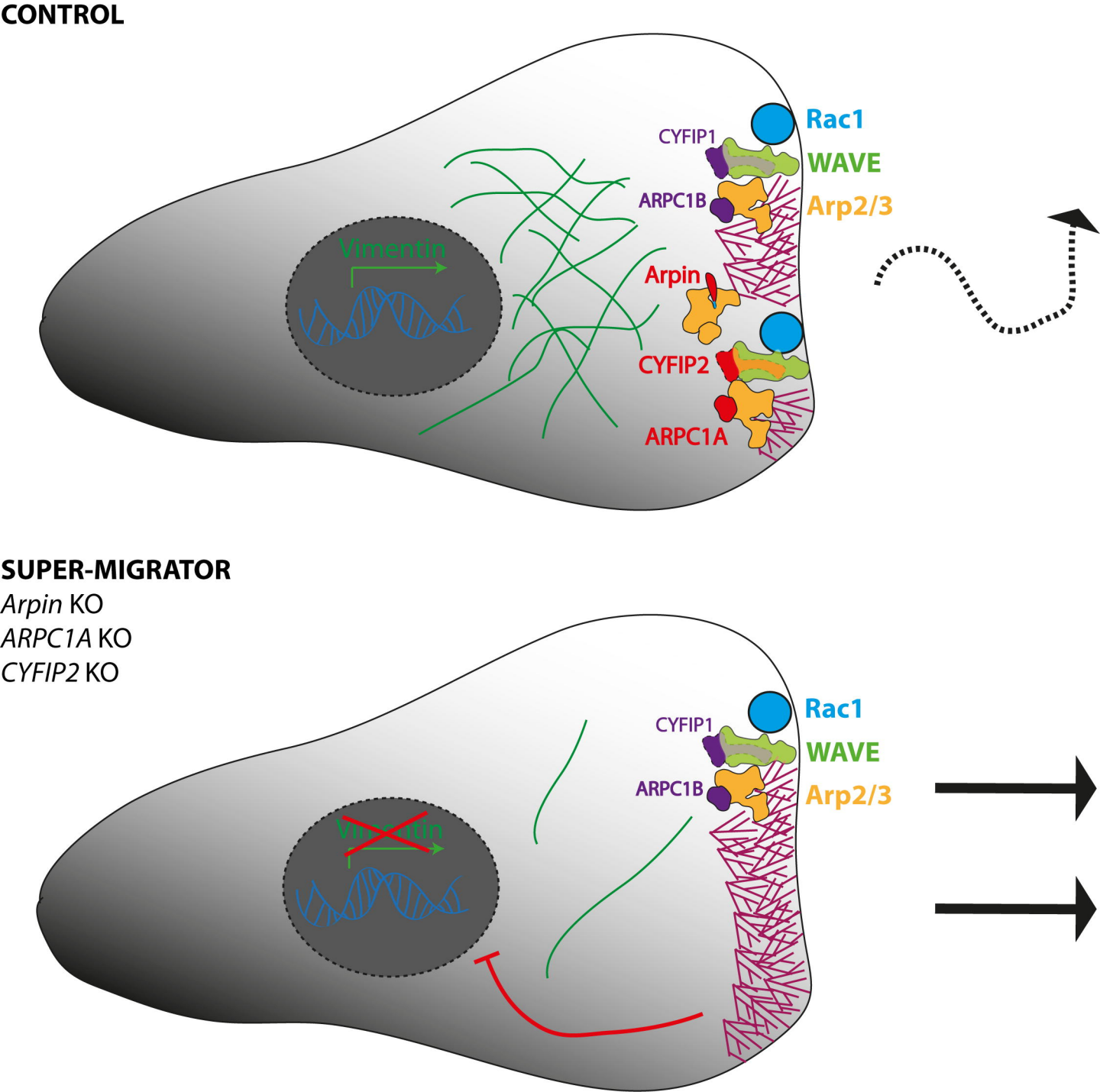
CONTROL
Rac1
CYFIP1
WAVE
ARPC1B
Arp2/3
Vimentin
Arpin
CYFIP2
ARPC1A
SUPER-MIGRATOR
Arpin KO
ARPC1A KO
CYFIP2 KO
Rac1
CYFIP1
WAVE
ARPC1B
Arp2/3